Supplemental material

Hofbauer et al., https://doi.org/10.1083/jcb.201802027

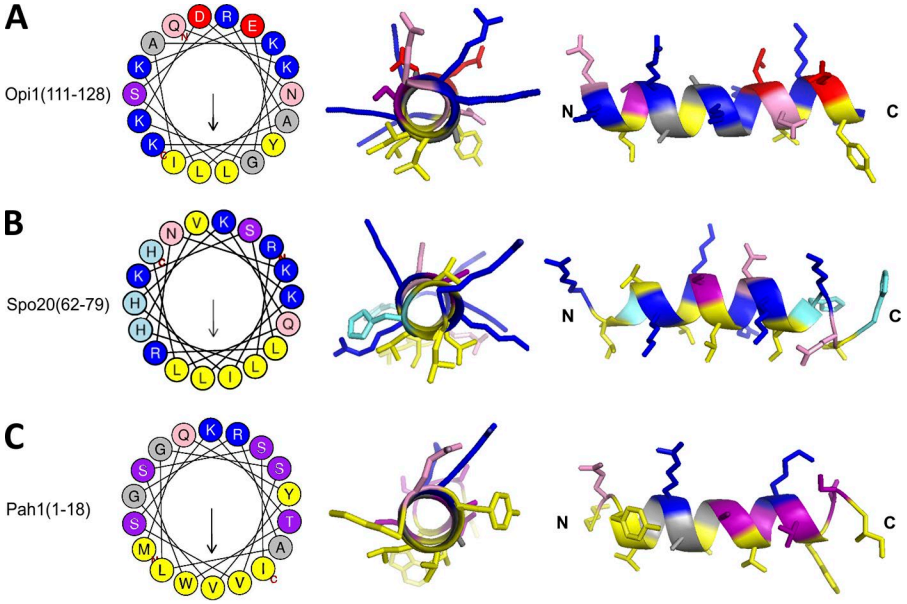

Figure S1. **Amphipathic helices of proteins sensing PA-rich membranes. (A–C)** Visualization of the AH of Opi1 (A), Spo20 (B), and Pah1 (C) using HeliQuest and PyMOL.

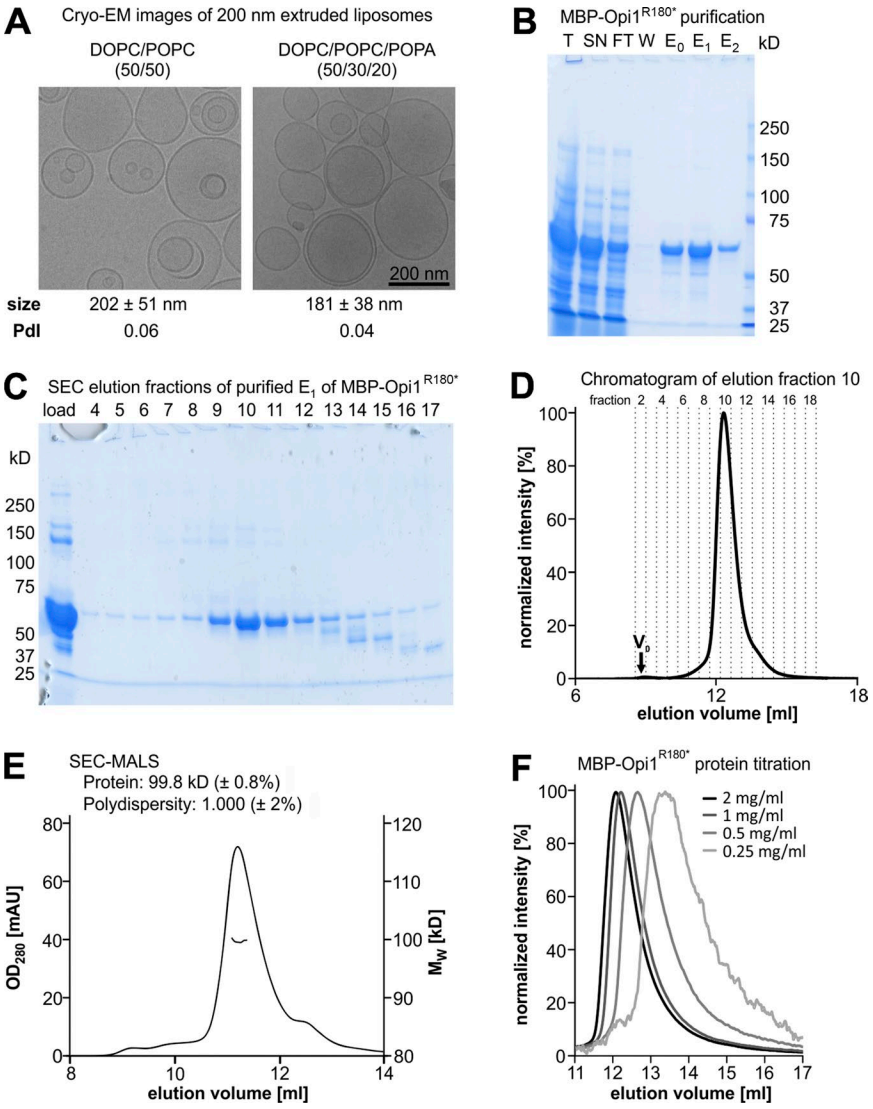

Figure S2. **Quality controls of purified MBP-Opi1^{R180*} variants and liposomes. (A)** Cryoelectron microscopic images of liposomes generated by extrusion through a 200-nm pore size polycarbonate filter. NanoSight measurements were performed to determine the mean size ± SD and the polydispersity index (PdI) of the extruded liposomes. **(B)** Purification of MBP-Opi1^{R180*}; SDS-PAGE of sample fractions from the affinity purification: total cell lysate (T), supernatant after centrifugation (SN), flowthrough (FT), wash (W), and elution (E) fractions from the affinity purification were subjected to the SDS-PAGE. **(C)** SDS-PAGE of SEC elution fractions from the affinity-purified elution fraction E_1 of MBP-Opi1^{R180*}. **(D)** Quality control of SEC-purified protein; SEC elution fraction 10 of MBP-Opi1^{R180*} was again subjected to SEC to verify good and stable protein quality. The void volume (V_0) of the Superdex 200 Increase 10/300 GL column was 8.9 ml. **(E)** SEC-MALS analysis was used to determine the average molecular mass and polydispersity of MBP-Opi1^{R180*}. **(F)** The dynamic equilibrium of MBP-Opi1^{R180*} was characterized by SEC experiments performed with different concentrations of MBP-Opi1^{R180*}.

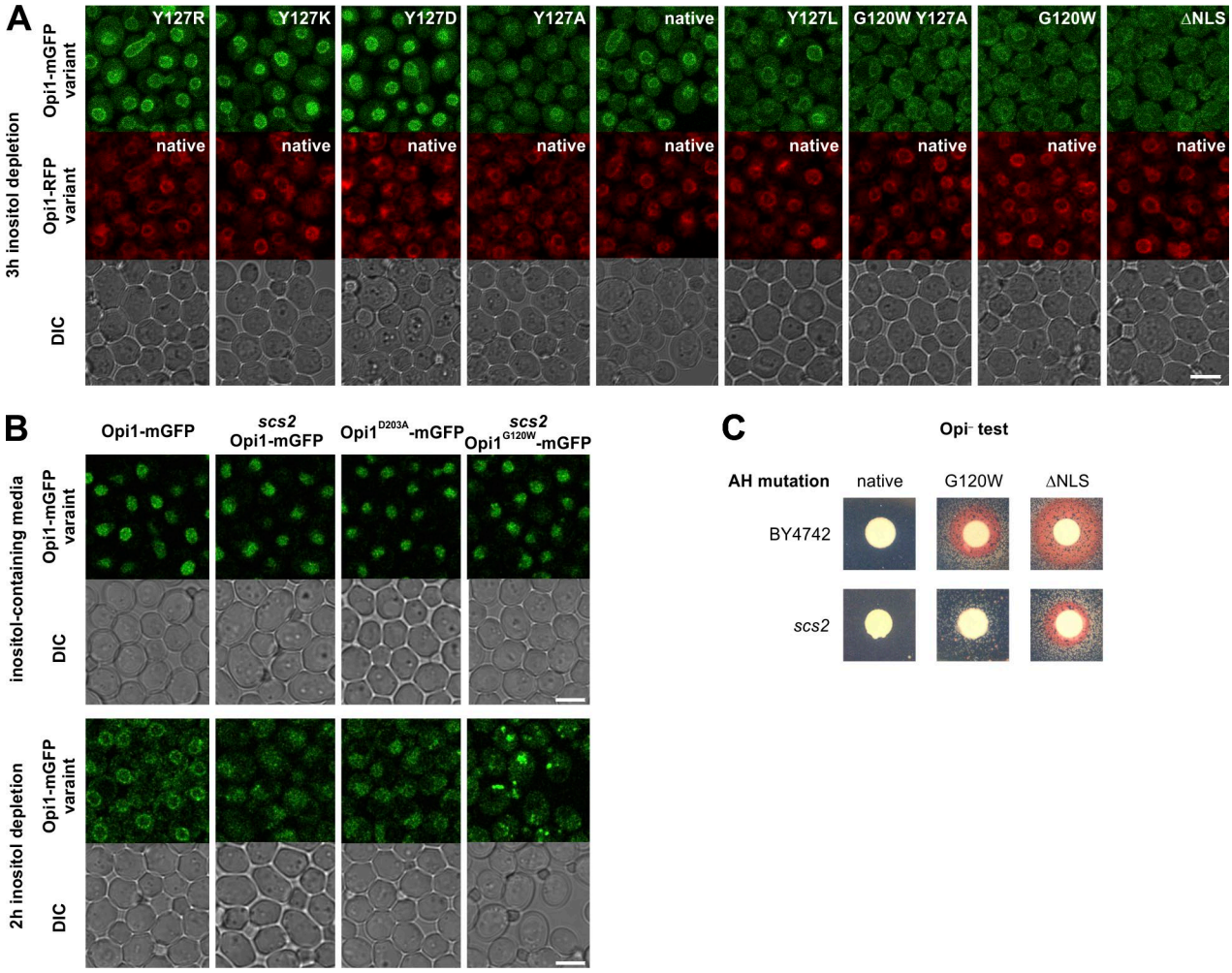

Figure S3. **Opi1 point mutations do not impair nuclear ER membrane binding of native Opi1 in diploid yeast cells. (A)** Representative microscopic images of diploid strains with chromosomally integrated Opi1-mGFP mutant variants as one allele and WT Opi1-mRFP as the other allele. The cells were cultivated and imaged 3 h after inositol depletion in liquid media. **(B)** Representative microscopic images of live cells expressing Opi1-mGFP variants in the WT and the *scs2* deletion strain background cultivated on inositol-containing liquid media or for 2 h after inositol depletion. Bars, 5 µm. DIC, differential interference contrast. **(C)** Opi⁻ phenotypes of the indicated Opi1-mGFP variants in the WT and the *scs2* deletion strain background.

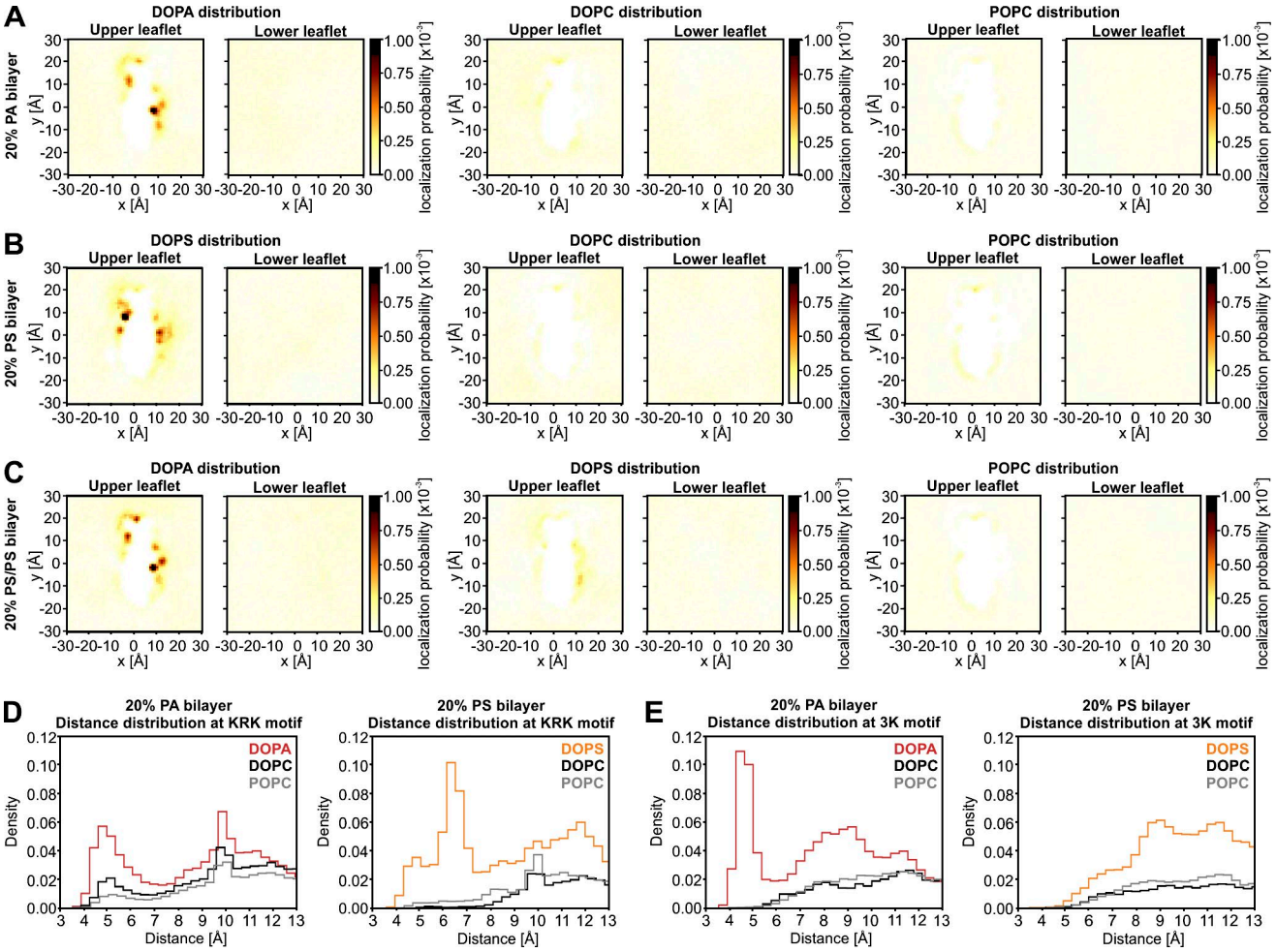

Figure S4. **Detailed results from MD simulations with the AH of Opi1. (A–C)** Time-averaged positions of phosphate head groups from different lipid species (DOPA, DOPS, DOPC, and POPC) in their respective all-atom MD simulations (A, 20% PA; B, 20% PS; C, mixed 20% PA/20% PS). Both membrane leaflets are shown: upper leaflet (Opi1 AH bound) and lower leaflet (unbound). Colors indicate the probability to observe a given lipid at that position over the course of the trajectory. DOPA and DOPS show enrichment at the 3K and KRK motifs in their respective simulations (A and B, left), whereas no enrichment is seen for DOPC and POPC (A and B, middle and right). DOPA displaces DOPS from both motifs in the mixed simulation (C, left and middle). **(D and E)** Distribution of pairwise distances calculated from a point of interest and all lipids of a given species in their respective simulations. **(D)** Distribution of lipids at the KRK motif for DOPA, DOPC, and POPC (left) and DOPS, DOPC, and POPC (right). **(E)** Distribution of lipids at the 3K motif for DOPA, DOPC, and POPC (left) and DOPS, DOPC, and POPC (right).

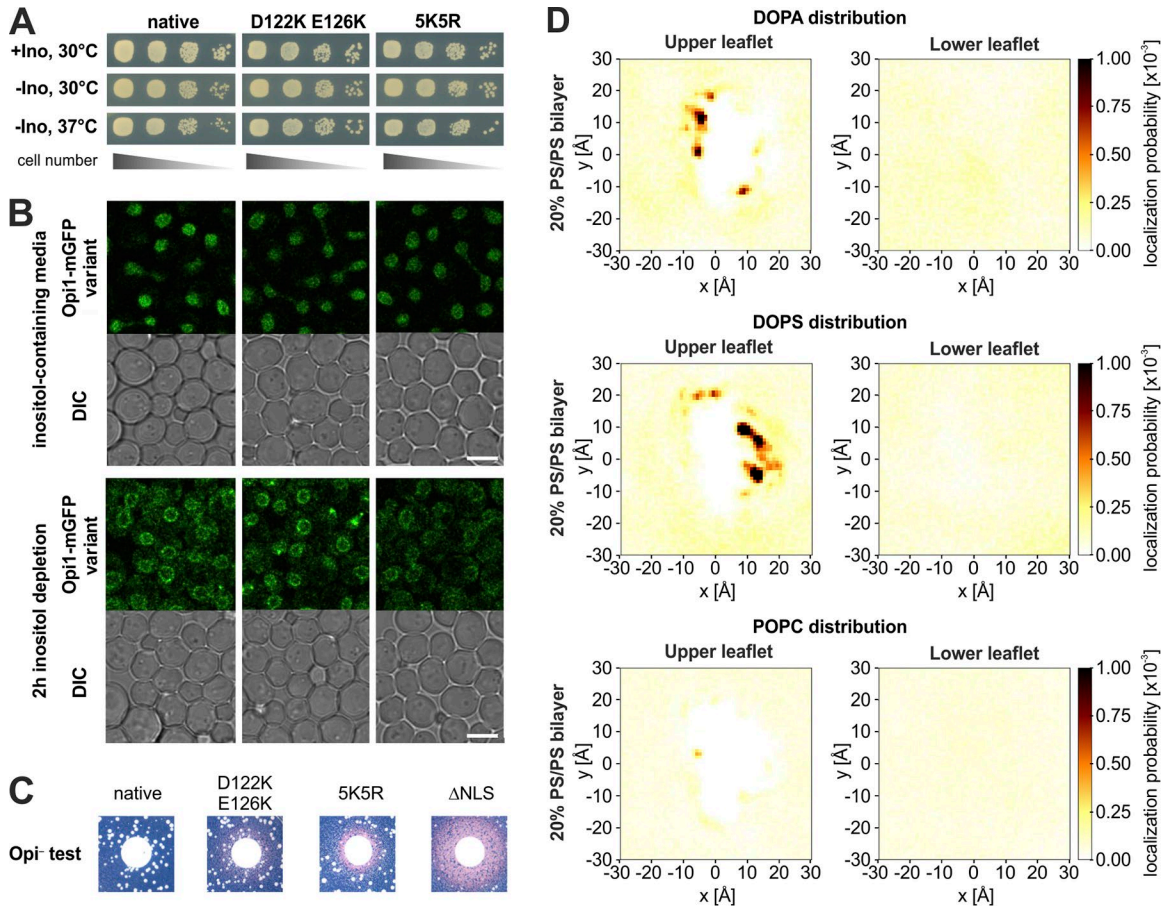

Figure S5. **Additional in vivo and MD simulation data reveal aberrant lipid selectivity of the 5K5R variant of Opi1. (A)** Viability assays of strains with chromosomally integrated Opi1-mGFP variants. Plates were scanned after 2 d cultivation on solid media either containing (+Ino) or lacking inositol (−Ino) at the indicated temperatures. **(B)** Representative microscopic images of live cells expressing Opi1-mGFP variants cultivated on inositol-containing liquid media or for 2 h after inositol depletion. Bars, 5 µm. DIC, differential interference contrast. **(C)** Opi⁻ phenotypes of the indicated Opi1-mGFP variants are monitored by a red halo from an inositol-auxotrophic tester strain around the spotted colonies. **(D)** Time-averaged positions of phosphate head groups from different lipid species (DOPA, DOPS, DOPC, and POPC) in an all-atom MD simulation of the 5K5R AH mutant peptides interacting with a mixed bilayer containing 20% PA/20% PS as represented in Fig. S4 C. In contrast with the AH derived from WT Opi1, the 5K5R AH efficiently recruits PS.

Table S1 is a separate PDF showing E. coli and S. cerevisiae strains used in this study.

Table S2 is a separate PDF showing plasmids used in this study.

Table S3 is a separate PDF showing primers used in this study.